Synthesis of NiO–CeO_2 nanocomposite for electrochemical sensing of perilous 4-nitrophenol

Naushad Ahmad, Manawwer Alam, Rizwan Wahab, Javed Ahmad, Mohd Ubaidullah, Anees A. Ansari & Nawaf M. Alotaibi

Journal of Materials Science: Materials in Electronics

ISSN 0957-4522
Volume 30
Number 19

J Mater Sci: Mater Electron (2019)
30:17643-17653
DOI 10.1007/s10854-019-02113-2

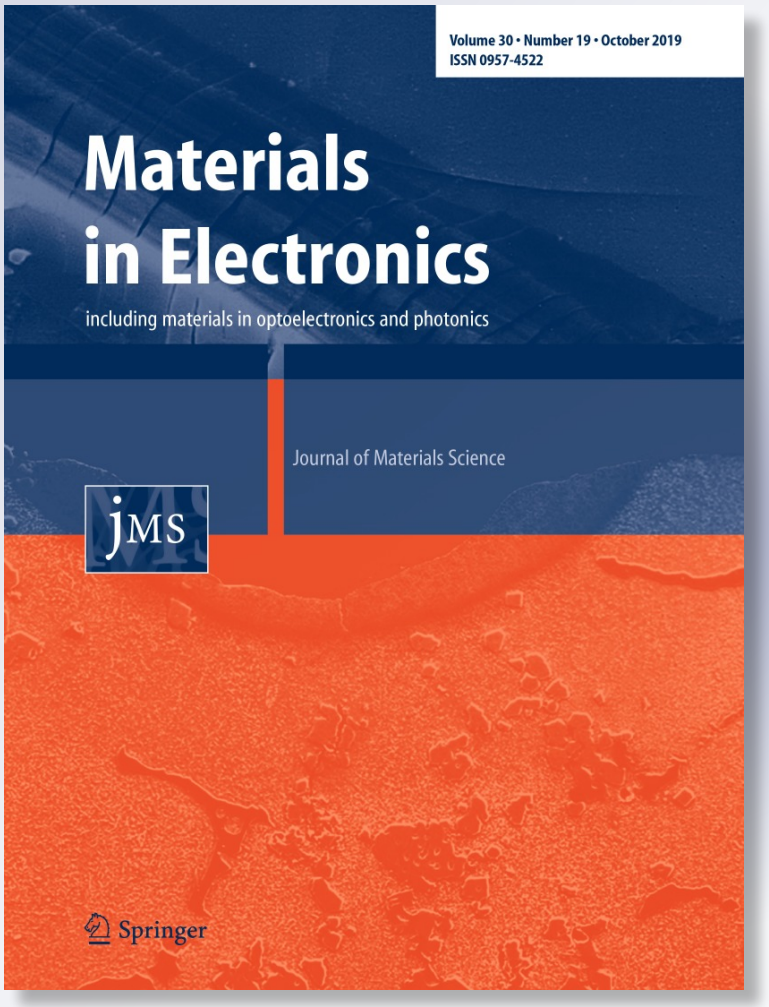

Springer

Journal of Materials Science: Materials in Electronics (2019) 30:17643–17653
https://doi.org/10.1007/s10854-019-02113-2

Synthesis of NiO–CeO_2 nanocomposite for electrochemical sensing of perilous 4-nitrophenol

Naushad Ahmad[1] · Manawwer Alam[1] · Rizwan Wahab[2] · Javed Ahmad[2] · Mohd Ubaidullah[1] · Anees A. Ansari[3] · Nawaf M. Alotaibi[1]

Received: 31 May 2019 / Accepted: 27 August 2019 / Published online: 5 September 2019

Abstract
Well-crystalline NiO–CeO_2 nanocomposites have been fabricated by ignition method and investigated by X-ray diffraction, Fourier Transform Infrared, UV–Vis diffuse reflectance spectroscopy, Thermal gravimetric analysis, BET surface area, and transmission electron microscopy. The detailed characterizations disclosed that the pre-calcine (700 °C) nanocomposite (NCC) has two pure phases: cubic fluorite phase (CeO_2) and cubic face-centered phase (NiO). Finally, the pre-calcine NCC nanocomposite was applied as electron intermediators for the electrochemical sensing of 4-nitrophenol (4-NP). Compared with as-grown modified electrode (NCG/GCE), pre-calcine electrode (NCC/GCE) exhibited more excellent conductivity and better electrocatalytic mediator for 4-NP. It was found that the NCC/GCE sensor displayed diffusion-controlled kinetics and excellent sensitivity (3.68 $A\mu M^{-1}$ cm^{-2}). The reduction current is directly proportional to the 4-NP concentration, ranging from 1 to 20 μM with lower detection limit of 2.48 μM.

1 Introduction

Phenolic compounds are very often exploited in manufacturing processes and to some extent unload into atmospheres [1]. Among phenolic compounds, nitrophenols and its derivatives (2-NP, 4-NP and 2-methyl-4-NP) are extensively used in the manufacturing of petroleum, insecticides, dyes, and medications. They are phylogenesis, discomfort, and biorefractory organic compounds and considered as harmful pollutants [2]. Among them, 4-NP is one of the most abundant and highly stable, and causes considerable damage to the surroundings and living systems [3]. In addition, its severe consumption by hominids can cause headaches, drowsiness, nausea, and cyanosis [4]. Since of toxic nature of nitrophenols, it was registered as a pollutant of the US Environmental Protection Agency [5]. So, the intensive monitoring and sensing of 4-NP has become critical for fortification of the environments. Numerous performances were testified for the identification of 4-NP, such as gas chromatography [6], liquid chromatography [7, 8], spectrophotometric [9], electrophoresis [10], flow and segmented injection techniques [11], and enzyme-linked immunosorbent analytical assay [12]. Then again, many of these methodologies are very complex, expensive, time consuming, and numerous kind of hazardous reagents and standards needs for testing environmental samples. Therefore, to develop a short time, sensitive and cost effective technique is of great importance for the determination and identification of 4-NP. Electrochemical techniques have prodigious ability for detection of various analytes because of the advantages of low-cost instruments, easy operation, high sensitivity, and handy sample treatment [13, 14]. In this research area, electrodes are key factor for the determination of analytes, however, the detection of analytes specifically 4-NP at unmodified electrodes shows low sensitivity, high overpotential, and faced various kinds of interference issues [15]. The ideal materials for electrodes must have excellence electron transport property, electrocatalytic activity, porosity, BET surface area, and high stability under suitable operating conditions. In order to implement, it is commonly useful to modify electrodes by suitable electrocatalytic materials. Then, the ideal properties of electrodes can be boosted according their types and structure of the material and also analyte to be detected.

✉ Naushad Ahmad
anaushad@ksu.edu.sa; naushaddrnaima@gmail.com

[1] Department of Chemistry, College of Science, King Saud University, Riyadh 11451, Kingdom of Saudi Arabia

[2] Department of Zoology, College of Science, King Saud University, Riyadh 11451, Kingdom of Saudi Arabia

[3] King Abdullah Institute for Nanotechnology, King Saud University, Riyadh 11451, Kingdom of Saudi Arabia

Therefore, for the detection of 4-NP, several kinds of chemically modified electrodes are widely used [16]. Producing a capable and competent electrochemical sensor for its detection has generated much curiosity among electrochemists. Although for the sensing of 4-NP with high life stability of modified working electrodes have been reported such as carbon nanotubes [17], metal nanoparticles [18, 19], and ionic liquids [20], but designing new composites with excellent electro catalytic features using a simpler preparation remains a challenge.

Metal oxide micro/nanostructures which have good optical and electrical properties received intensive attention in electrochemistry. These are the promising materials for the immobilization of different electron transfer mediator molecules and biomolecules because of their high conductivity, surface to area ratio, wide ranging electrochemical working window, excellent substrate attraction, significant mechanical strength, and steady stable electrochemical properties [21–23]. Controlling of compositions, size, morphology and metal doping are considered as a proficient approach to modify the electrocatalytic task of metal oxides. Metal doping is a prominent tool to alter the structural, optical, and electrical-sensing parameters which in turn provide extended interface for various sensing devices. In addition, it is very important to recognize the outcomes of dopant concentrations on electrocatalytic and structural properties. Many scientists successfully applied limited available high price noble metals and its doped metal oxides in order to enhance the electrocatalytic activity, but it desirable to search for new alternatives with more earth-abundant metals, such as Co, Ni or Ce [24–26]. Among the metal oxides, composites of cerium oxide have high mechanical strength, optical property, biocompatibility, nontoxicity, oxygen ion conductivity, high thermal stability, and wide range of applications [27–30]. These properties are much applicable for many analytes such as phenols [31], CO [32], ethanol [33], and H_2O_2 [34]. Low electrocatalytic activity and stability and are the main drawbacks against commercial applications of the transition metals. Among the transition metals, nickel is commonly used as an electro-catalyst for surface redox reactions in many applications [35, 36]. The doping of nickel oxide (NiO) is motivated electrocatalytic activity through the synergistic benefit and induced electron transfer from the combined properties of the components [35, 36]. Similar composites was also prepared and presented by Ranjbar et al. [37] and it showed the formation of Mg-MOF-74 synthesized successfully through microwave method with using 2,6-pyridinedicarboxylic acid [37]. In other report, hollow sphere-like $ZnS/ZnAl_2S_4$ nanocomposites were formed via solvo thermal process and characterized [38]. To this continuation, the rod shaped zinc oxide nanostructures were formed and to this formation pomegranate juice was used as capping agent for self-assembly of nanostructures [39]. The NiO nanoparticles were processed via solventless route by solid-state thermal decomposition and physico chemical characteristic were well characterized [40]. The copper, tungsten and nickel ($Cu(WO_4)$ nanoparticles) based nanocomposite were prepared and photocatalytic activity were accessed with methyl orange (MO) dye [41]. The cerium-doped copper ferrite nanoparticles ($CuFe_{2-x}Ce_xO_4$) through an auto-combustion method and were used as photocatalyst application [42]. The novel $MnWO_4/TmVO_4$ ternary nano-hybrids were fabricated via sonochemical method and were used for the degradation with different dyes such as rhodamine B (RhB), 2-naphthol (Na), phenol red (PhR), and eosin Y(EY) under visible light for photocatalytic study [43]. Over various properties, the nano composites materials were largely used as an electrochemical sensor such as the cerium tungstate nanostructures were prepared and their supercapacitive properties were accessed via electrochemical studies [44]. The copper carbonate nanoparticles were used as an anode material, formed via solid-state thermal decomposition reaction [45]. The terbium tungstate (TWNPs) nanocomposite nanoparticles were also prepared via sonochemical method and used as electrode materials and applied as hybrid vehicle systems [46].

In present work, we have systematically investigated the structural, thermal, optical, and sensing properties of $NiO–CeO_2$ nanocomposites (NCCs) by various physio chemical properties. The NCCs were prepared by self-combustion method and were characterized through XRD, TEM, TGA, FT-IR, UV/Vis-DRS and BET surface area. Further, cyclic voltammetry (CV) has been used for the investigation of the electro chemical properties and electrocatalytic activity of the nanocomposite-modified electrode.

2 Experimental

2.1 Synthesis of NiO/CeO_2 (NC) nanocomposite

Entire chemical reagents were analytical grade and used as received without any further purification/modification. The NC nanocomposites were synthesized by solution combustion method using glycine as a fuel and metal nitrates as oxidizer. In a typical reaction process, equimolar amounts (0.5 mol L^{-1}) of cerium nitrate (99.99%, BDH Chemicals Ltd, England) and nickel nitrate (99.99%, E-Merck, Germany) were added into 250 mL round bottom flask containing appropriate amount of glycine fuel. The resultant mixture was stirred at 90 °C for 1 h. Afterwards; the filtrate mixture was transferred to a ceramic dish, which was placed in a preheated muffle furnace at 300 °C. During heating, the mixtures self-ignited and form highly spongy materials. The obtained material was washed with water, ethanol, and acetone. Further, it was annealed at 300 °C, 500 °C and

700 °C for 5 h in nitrogen gas at the heating rate of 5 °C min^{-1}. The annealing temperature was used for the determination of crystallinity which in turn an important factor for sensing of the processed powder.

2.2 Characterizations of NiO/CeO_2 (NC) nanocomposite

The crystal phases of the prepared powders were recorded via Rigaku diffractometer (Shimadzu XD-3A, Japan) using filtered CuK_α radiation ($\lambda = 0.15405$ nm). The thermal decompositions of the precursor was performed by using Mettler Toledo TGA/DSC 1 STARe thermal analyzer (Switzerland) between 50 and 900 °C at the heating ramp of 20 °C min^{-1} in flow of nitrogen. The chemical composition was recorded on FTIR spectroscopy in the range of 400–4000 cm^{-1}. Microstructure of the NCC nanocomposite was inspected by means of a TEM (JEM-2100F, JEOL, Japan) operating at an accelerating voltage of 200 kV. The purity of nanocomposite material/elemental composition was analyzed with the use of energy dispersive spectroscopy (EDS), equipped with the provision of scanning electron microscopy (SEM) at room temperature (JEOL, JED-2200 series, Japan). The BET surface areas of calcined catalyst were measured on a Micromeritics TriStar 3000 apparatus by the N_2 adsorption isotherm at 77 K. Sample degassing was carried out at 300 °C prior to acquiring the adsorption–desorption isotherm. UV-DRS were recorded via Hitachi U-3410 spectrophotometer from the wave length range 200–800 nm, using optical-grade $BaSO_4$ powder as a reference. All pH measurements were accomplished with a pH-Meter PB-10 (Sartorius, Germany).

2.3 Electrochemical measurement of 4-NP

The electrochemical measurements have been carried out by Metrohm autolab PG electrochemical system (Netherlands). Cell of three electrode system was fabricated using, GC working electrode (surface area: 0.071 cm^2), Pt auxiliary electrode and Ag/AgCl/(sat 3MKCl) reference electrode. The working electrode was made-up by coating the paste of prepared electrocatalysts and binder on GCE, polished with 0.5 µm alumina–water slurry. For the coating, a viscous paste of nanocomposites was prepared with ethyl cellulose binder with an appropriate ratio (70:30) and coated on polished electrode and it was dried overnight in air at room temperature. The electrodes are named NCG/GCE and NCC/GCE for as grown and pre-calcine composite at 700 °C, respectively. All sensing measurement were carried out in N_2-saturated PBS solution (0.01 M) at room temperature in absence and presence of 4-NP.

3 Results and discussion

3.1 XRD analysis

Figure 1 display influence of calcination temperature on the prepared composite for the arrangement of crystal structure. It was observed that the powder calcined at 300 °C and 500 °C temperature exhibited wide and diffuse peaks, which designate small crystallites and disordered structure. Furthermore, the peak sharpness and intensities seemingly improved with increase of calcination temperature, by particle sintering, crystal ordering, and crystallite growth. Before the calcinations, the sample seemed to be contained CeO_2 (28.7° and 47.4°) and NiO (37.2° and 63.2°) diffraction peaks. After calcinations (500 and 700 °C), sharp diffraction peaks observed at 28.7° (111), 33.1° (200), 47.4° (220), 56.4° (311) 59.3° (222), 69.8° (400) 76.9° (331) and 79.3° (420) corresponded to the diffraction peaks of CeO_2. These peaks imply that CeO_2 exhibits a cubic fluorite structure [47]. In addition, three other peaks are observed at 37.2° (111), 43.5° (200), and 63.2° (220) in the nanocomposite correspond to face-centered cubic phase NiO [48]. There are no other phases are detected, indicating that the product is of high purity. The characteristic diffraction peaks related to the CeO_2 and NiO phases are matched with JCPDS card

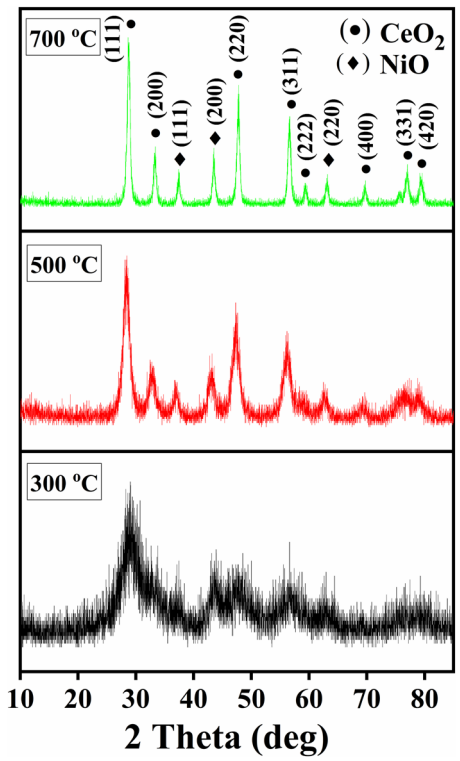

Fig. 1 XRD patterns of the NiO–CeO_2 nanocomposites calcine at various temperatures

no. 01-075-0076 and 01-078-0429, respectively. The most intense peak is (111) for CeO_2 and (200) for NiO. The crystalline size of most intense peak, (111) for CeO_2 and (200) for NiO was calculated by Scherrer's formula and founded ~ 10 nm and 15 nm, respectively. It is indicative that the pre-calcine nanocomposite (NCC) at 700 °C is desired for electrochemical sensing of 4-NP.

3.2 Thermal study of the precursor

Figure 2 displayed the TG-DTG peak profile of the fabricated precursor. There are two mass loss appeared in TGA graph; the first mass loss below 250 °C, and is described by a small and weak DTG peak at 155 °C and second pronounced mass loss between 250 to 600 °C, and its described by a wide and strong DTG peak at 415 °C. The mass loss below 250 °C is described the thermal degradation of physical adsorbed solvents, moisture and nitrate ions (~ 5% mass loss). The second mass loss between 300 to 600 °C can be attributed to the combustion type decomposition of free glycine and glycine complexes followed by solid state reactions (~ 29% mass loss).

3.3 FTIR spectroscopic analysis

In order to identify the functional characteristics of synthesized sample at different heat treatment it was examined by FTIR spectroscopy. Figure 3 demonstrated through various well-defined absorption peaks at 3425, 2923, 2345, 1618, 1365, 881, 555 and 470 cm^{-1} of synthesized nanocomposites. It was observed that peaks become small with increasing calcination temperature. The presence of three absorption bands at 3425, 2923 and 1617 cm^{-1} were attributable to stretching and bending vibration of surface hydroxyl or adsorbed water and carbonation on the surface of NiO–CeO_2 nano structures from surroundings, respectively [49–51].

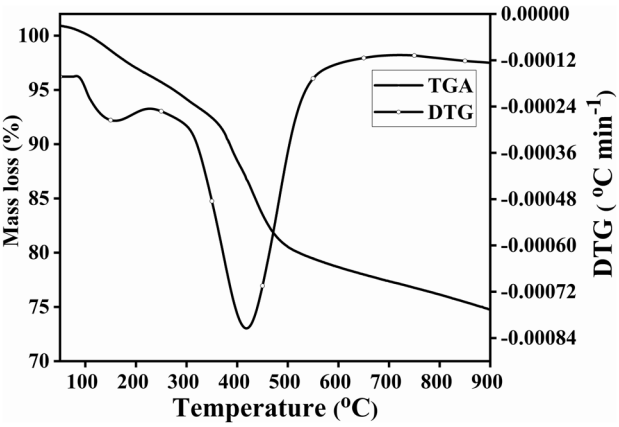

Fig. 2 TG and DTG curves of NiO–CeO_2 precursor

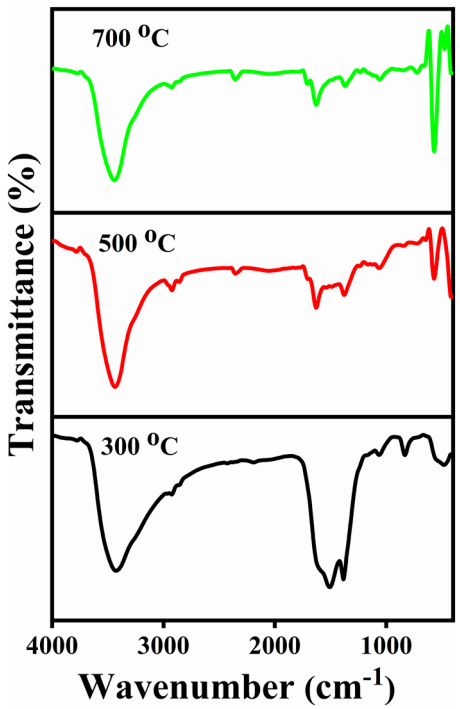

Fig. 3 FTIR spectra of NiO–CeO_2 nanocomposite at different temperature

The presence of sharp and strong absorption peak appeared at 555 and 470 cm^{-1} is demonstrated the formation of metal-oxide (M–O) bonds and confirmed that the formation of nanocomposite of NiO–CeO_2 [52–54]. The appearance of two small absorption peaks at 1365 and 881 cm^{-1} are due to the presence of nitrate group.

3.4 Optical properties

Optical properties of the produced NiO–CeO_2 NCs were examined by UV–Vis in DRS mode. Figure 4 reveals that the absorption spectra and its corresponding band gap energies at different temperature (300, 500 and 700 °C) the synthesized nano composite. It was found that the as-prepared sample show one broad peak and calcine composite display two peaks in visible range, Fig. 4a. This result suggests that all composites are potential candidate for photocatalytic applications in visible region. The presence of two distinctive absorption peaks in calcine samples confirms the formation of nano composite due to the presence of both NiO and CeO_2 nanoparticles, which are good agreement with XRD data. In addition, the absorption band shifted towards visible region with an increase of calcination temperature.

The optical energy was calculated by Tauc's equation:

$$\alpha h\nu = A\left(h\nu - E_g\right)^n$$

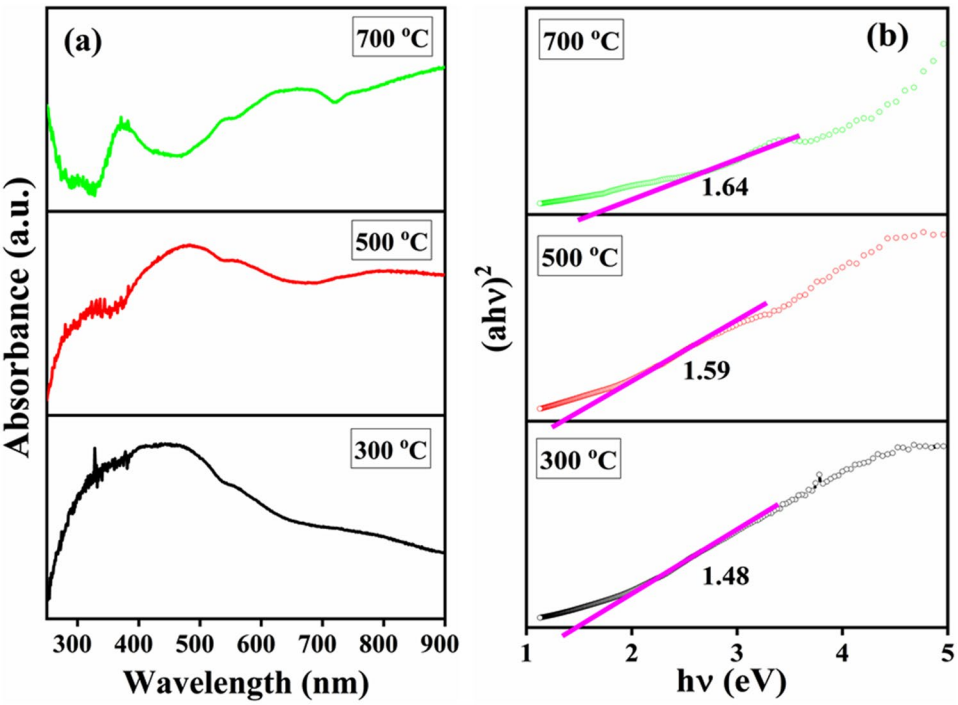

Fig. 4 **a** UV–Vis absorption spectra **b** plots of $(\alpha h\nu)_2$ as function of energy of NiO–CeO_2 nanocomposite at different temperature

where α, h, ν, E_g and A are absorption coefficient, Planck's constant, photon frequency, optical band gap energy, and a constant, respectively, and 'n' is based on the nature of optical transition of a semiconductor [55]. Figure 4b illustrate a plot between $(\alpha h\nu)^2$ and hν. The tangent lines were drawn to determine the band gaps of the synthesized catalysts. The calculated band gap energy of samples was increased gradually with temperature from 1.48 to 1.64 eV with calcination temperature, which is smaller than the value for bulk of CeO_2 (3.19 eV).

3.5 Morphological and porosity measurements

The morphology of NCC nanostructures were analyzed via the TEM images at room temperature and presented as in Fig. 5, under high Fig. 5a and low Fig. 5b magnifications scales. From the obtained images, it is observed that the majority of NCC particles are composed of well dispersed nanocubes. The acquired data reveals that the average size of each cubes are ~ 20 ± 5 nm. Small grown NPs, when sintered at high temperature are comes closer due to high energy and to form a cubes shaped nanostructures. The average particle diameter of each nanocube (~ 20 ± 5 nm) is in very close and consistent with the XRD analysis.

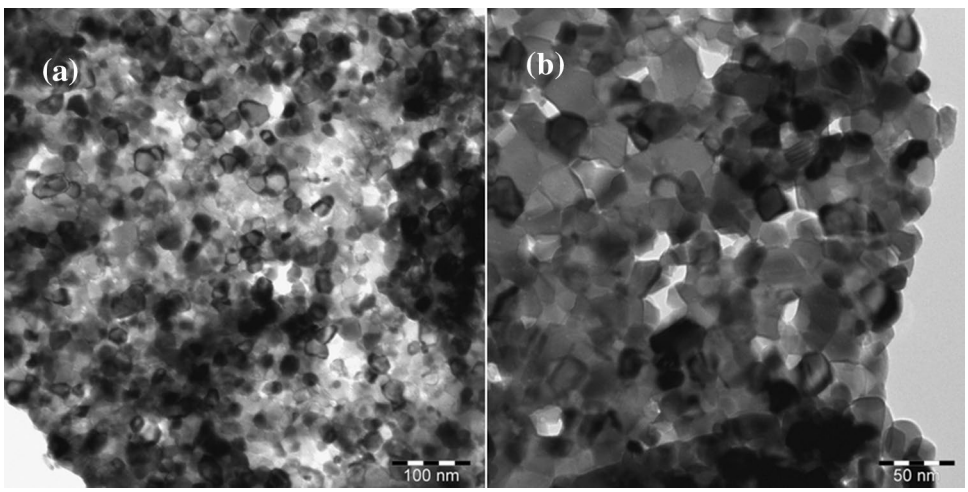

Fig. 5 Morphology of NCC nanocomposite at low (**a**) and high (**b**) magnification

The nitrogen sorption isotherm and pore-size distribution curve for the NCC powder is presented on Fig. 6. This isotherm is the characteristic of adsorption–desorption of mesoporous solids (Fig. 6a). According to IUPAC classification, isotherm represents type IV isotherm and H3 shaped hysteresis loop with relative pressure in a range of $0.6 < P/P0 < 0.98$, implying appearance of ordered mesoporous structure, which was caused by accumulation of NPs [56, 57]. The BET surface area, mesopore volume and average pore size were found 15.82 $m^2\ g^{-1}$, 0.085 $cm^2\ g^{-1}$ and 21.92 nm, respectively. Figure 6b, shows the couple of mesoporous centered at 11.60 and 46.10 Å, indicates that this calcine sample possess double porous framework.

The elemental composition of annealed (at 700 °C) sample of NiO–CeO_2 nanocomposite was examined by EDS spectroscopy at a specified area shown through SEM image (Fig. 7a, b). The elemental analysis (EDS spectrum) shows that only nickel (34.70%), cerium (65.30%) appeared in the spectrum and this depicts that the formed nanocomposite structures were synthesized through the nickel and cerium salt. There are no other organic impurities such as byproduct or other element was found in the spectrum, which again justifies that the synthesized nanocomposite (NiO–CeO_2) structures are highly pure.

3.6 Electrochemical properties of modified electrodes

3.6.1 Preliminary test

Cyclic voltammetry (CV) experiments were performed to test the electrochemical properties of the NCs electrodes in 0.01 M PBS solution (pH 7.4) to finalized the detection of 4-NP. Electrochemical performances for the bare and modified electrodes in absence and presence of 4-NP of as-grown and pre-calcined sample at 700 °C were examined over the potential range from −0.1 to +1 V at a scan rate of 100 mV s^{-1} and obtained CV profiles are shown in Fig. 8. It can be observed that calcine electrode (NC C/GCE) exhibited better electrocatalytic activity than bare GCE and as-grown electrode (NCG/GCE) in presence of 4-NP. It is also observed that in absence of 4-NP modified (NCC/GCE) electrode showed higher electrocatalytic behavior than (NCG/GCE) in presence of 4-NP. It can be noted that in presence of 4-NP, (NCC/GCE) modified electrode showed broad cathodic peak at 0.38 V (vs. Ag/AgCl), an irreversible reduction of the nitrogroup to the corresponding hydroxylamine group. An obvious increase of currents suggests the higher electrocatalytic behavior of (NCC/GCE) electrode which may be attributed to the excellent conductivity and presence of different nature of the reactive sites onto the electrode surface. No redox peak was observed on the bare GCE and (NCG/GCE) surface in presence of 4-NP, possibly due to the unfavorable orientation of molecules on the electrodes surface and owing to its limited electrical conductivity. Therefore, the smallest size of NC nanocomposite calcine to 700 °C was chosen for subsequent detection of 4-NP.

3.6.2 Effect of concentration

The CV of NCC/GCE electrode in 0.01 M buffer in presence of different concentrations (1–20 µM) 4-NP were recorded at a scan rate of 100 mV s^{-1} and the consequences are shown in Fig. 9a. Each cyclic voltammetric response demonstrate a sigmoidal curve roughly, indicating the presence of a steady-state diffusion-limited current. It is clearly seen that the electrochemical reduction peak currents increase with 4-NP concentration. The peak became more and more pronounced and potential shifted right with increasing of 4-NP concentration and it implying that the NCC/GCE can effectively catalyze the electro chemical reduction of 4-NP.

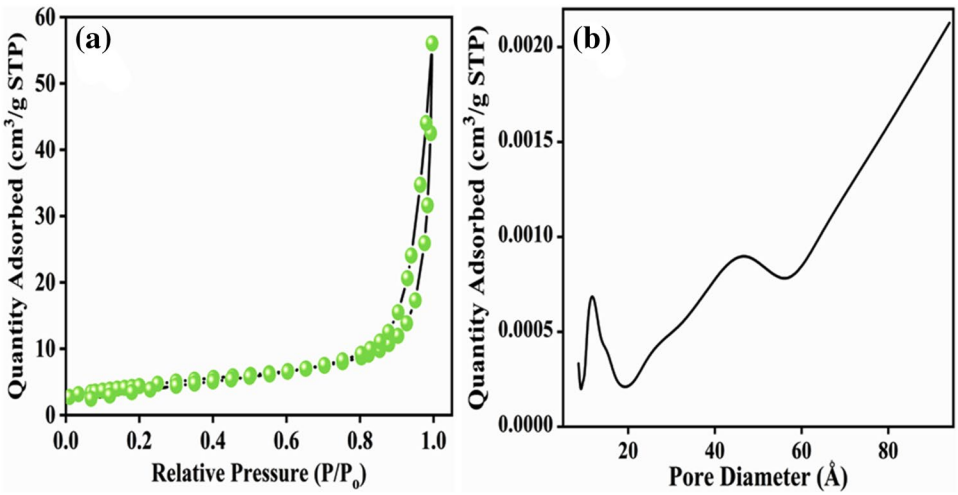

Fig. 6 Adsorption–desorption isotherm (**a**) and BJH plot (**b**) for NCC nanocomposite

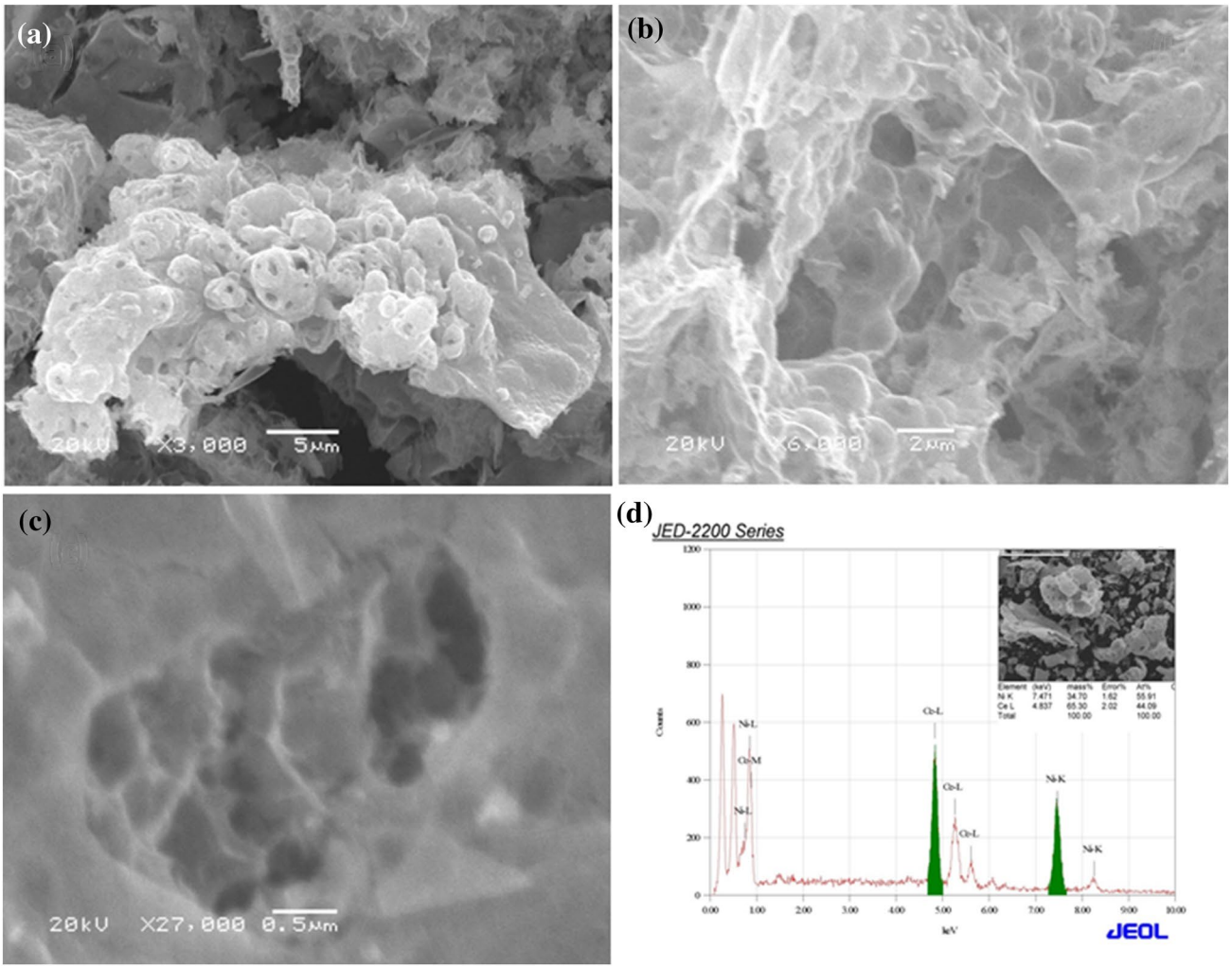

Fig. 7 Low (**a** & **b**) and high (**c**) magnified SEM images and their EDS of NCC nanocomposite

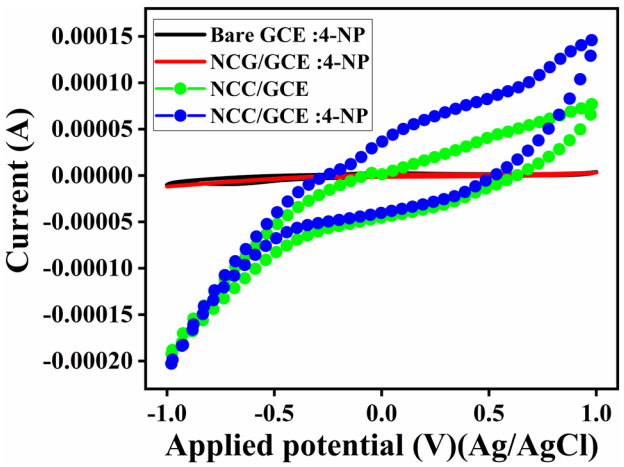

Fig. 8 Cyclic voltammetry responses of modified electrodes in the absence and presence of 4-NP (4 μM) in 0.01 M phosphate buffer (pH 7.4). Scan rate: 100 mV s^{-1}

The calibration curve deduced from reduction peak current verses 4-NP concentration is shown in Fig. 9b. The NCC/GCE electrode gives a linear response which suggest a diffusion controlled process [58]. The sensitivity was calculated from the slope of calibration curve, which was found to be 3.69 $A\mu M^{-1}$ cm^{-2}. The detection limit for the developed sensor as estimated (LOD = 3.3σ/Slope) from this curve is 2.48 μM.

3.6.3 Effect of scan rate

In order to recognize the kinetics of the electrochemical process, CVs were carried at various scan rates. Figure 10a elucidates the influence of scan rate on the current of 4-NP (4 μM) at NCC/GCE in 0.01 M PBS. It is observed that with increasing the scan rate, the reduction peaks current (Ip_c) increases correspondingly and peaks are shifted toward more negative potentials suggest that the reduction process

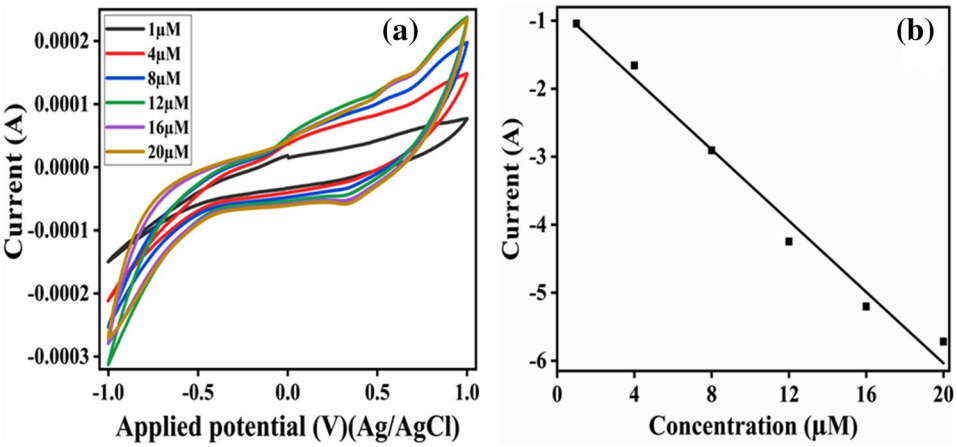

Fig. 9 **a** Cyclic voltammetric responses of NCC modified electrode as a function of 4-NP concentration. **b** Calibration curve between 4-NP concentration and magnitude of peak current. Scan rate: 100 mV s^{-1}

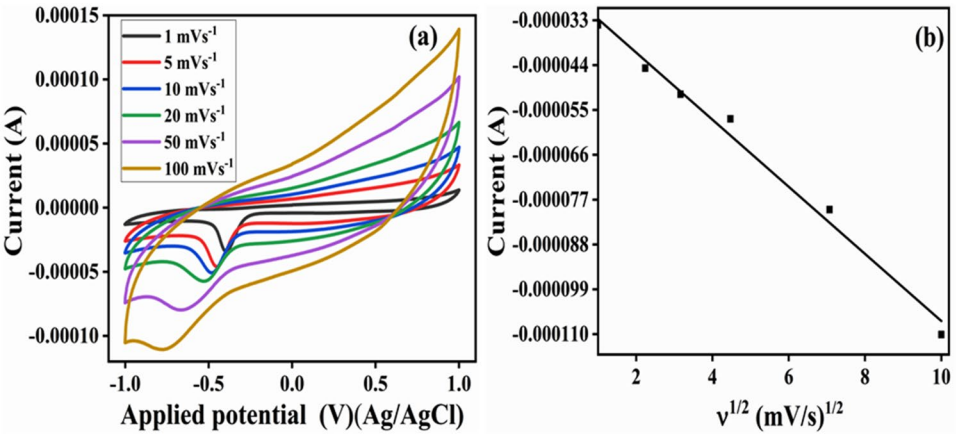

Fig. 10 **a** Cyclic voltammetric responses of NCC modified electrode in the presence of 4-NP (4 μM) as a function of at different scan rates. **b** Linear dependence of peak current with the square root of scan rate

occurred at the surface of electrode is diffusion controlled and irreversible. Figure 10b shows a plot of cathodic peak current against the square root of the scan rate which exhibits a linear relationship between the two parameters that again confirms the occurrence of diffusion-controlled electron transfer process on the CNN/GCE surface [59]. The linear regression equation is $Ip_c = -8.23 \times 10^{-6} + (-2.44 \times 10^{-5}$ $\nu^{1/2}$ $(mV/s)^{1/2}$. The correlation coefficient (r^2) was found to be 0.995.

3.6.4 Reproducibility and stability of the sensor

The reproducibility and stability of the fabricated sensor were also evaluated. Figure 11 shows the five consecutive cycles the NCC/GCE electrode in presence of 4-NP (4 μM) in 0.01 M PBS. The sensor shows an excellent reproducibility over five consecutive measurements in presence of 4-NP. The observed relative standard deviation (RSD) was found to 2.6%, which confirmed that the prepared electrode possessed satisfied reproducibility. The long-term stability of the sensor was also evaluated (inset Fig. 11). Tests carried out first day and after 45 days, during which the sensor was stored at ambient conditions, and showed only a little change in shape

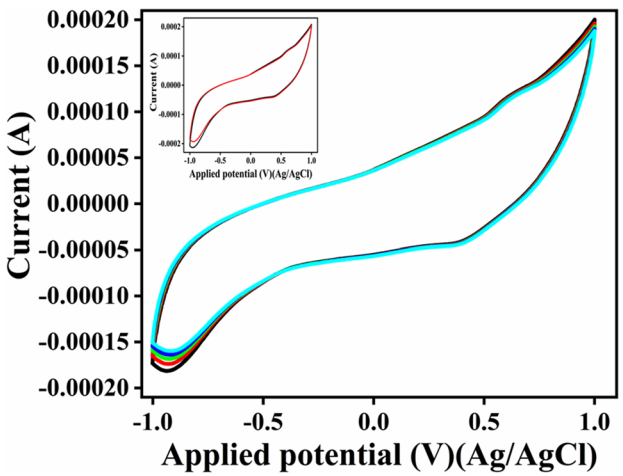

Fig. 11 Five consecutive cycles for the sample in presence of 4 μM (4-NP) in 0.01 M PBS at 100 mV s^{-1}, inset: stability test first and after 45 days at the same conditions

of the voltammetric cycle with a difference of the reduction current of about 4.49% compared to its initial value, confirming a good long-term stability. These results confirm

that the NCC/GCE electrode has a high stability as well as good reproducibility makes it applicable for practical use.

4 Conclusions

In the present work, we have successfully synthesized NiO–CeO_2 nanocomposites via solution combustion method by using glycine as the fuel and metal nitrates as oxidizers. The prepared materials were well characterized using many techniques such as X-ray diffraction pattern (XRD), transmission electron microscopy (TEM), UV–Visible diffused reflectance (UV-DRS) and Fourier transform spectroscopy (FTIR) to study the structural, morphological, optical, and surface functional properties respectively. These analyses have been identified as good candidates for electrochemical detection of prepared 4-NP. The simply fabricated calcine nanocomposite at 700 °C electrochemical sensor showed superior electrochemical performance for the determination of 4-NP relative to as-prepared and bare electrodes. The effect of concentration and scan rate variation on the electrochemical activity was also investigated. The prepared electrode showed excellent stability, reproducibility, and electrocatalytic activity towards the reduction of 4-NP with a high sensitivity (3.68 $A\mu M^{-1}$ cm^{-2}) and a low detection limit (2.48 μM) with a wide linear range (1–20 μM).

Acknowledgements The authors extend their appreciation to the Deanship of Scientific Research at King Saud University for funding this work through research group no. RG-218.

References

1. A.L. Buikema, M.J. McGimres, J. Cairns, Phenolics in aquatic ecosystems: a selected review of recent literature. Mar. Environ. Res. **2**, 87–181 (1979)
2. C. Schummer, C. Groff, J.A. Chami, F. Jaber, M. Millet, Analysis of phenols and nitrophenols in rainwater collected simultaneously on an urban and rural site in east of France. Sci. Total Environ. **407**, 5637–5643 (2009)
3. P. Wang, J. Xiao, A. Liao, P. Li, M. Guo, Y. Xia, Electrochemical determination of 4-nitrophenol using uniform nanoparticle film electrode of glass carbon fabricated facilely by square wave potential pulses. Electrochim. Acta **176**, 448–455 (2015)
4. X.M. Xu, Z. Liu, X. Zhang, S. Duan, S. Xu, C.L. Zhou, Cyclodextrin functionalized mesoporous silica for electrochemical selective sensor: simultaneous determination of nitrophenol isomers. Electrochim. Acta **58**, 142–149 (2011)
5. S.S. Li, D. Du, J. Huang, H.Y. Tu, Y.Q. Yang, A.D. Zhang, One-step electrode-position of a molecularly imprinting chitosan/phenyltrimethoxysilane/AuNPshybrid film and its application in the selective determination of p-nitrophenol. Analyst **138**, 2761–2768 (2013)
6. J.A. Padilla-Sanchez, P. Plaza-Bolanos, R. Romero-Gonzalez, N. Barco-Bonilla, J.L. Martin ez-Vidal, A. Garrido-Frenich, Simultaneous analysis of chlorophenols, alkyl phenols, nitrophenols and cresols in waste water effluents, using solid phase extraction and further determination by gas chromatography-tandem mass spectro metry. Talanta **85**, 2397–2404 (2011)
7. R.J. Chung, M.I. Leong, S.D. Huang, Determination of nitrophenols using ultra- high pressure liquid chromatography and a new manual shaking-enhanced, ultra sound-assisted emulsification microextraction method based on solidification of a floating organic droplet. J. Chromatogr. A **1246**, 55–61 (2012)
8. M.C. Alcudia-Leon, R. Lucena, S. Cardenas, M. Valcarcel, Determination of phenols in waters by stir membrane liquid-liquid-liquid microextraction coupled to liquid chromatography with ultraviolet detection. J Chromatogr. A **1218**(2176–21), 81 (2011)
9. F. Bagheban-Shahri, A. Niazi, A. Akrami, Simultaneous spectrophotometric determination of nitrophenol isomers in environmental samples using first derivative of the density ratio spectra. J. Chem. Health Risks **2**, 21–28 (2012)
10. X.F. Guo, Z.H. Wang, S.P. Zhou, The separation and determination of nitrophenol isomers by high-performance capillary zone electrophoresis. Talanta **64**, 135–139 (2004)
11. M. Manera, M. Miró, J.M. Estela, V. Cerdà, M.A. Segundo, J.L.F.C. Lima, Flow-through solid-phase reflectometric method for simultaneous multiresidue determina- tion of nitrophenol derivatives. Anal. Chim. Acta **600**, 155–163 (2007)
12. S. Tingry, C. Innocent, S. Touil, A. Deratani, P. Seta, Carbon paste biosensor for phenol detection of impregnated tissue: modification of selectivity by using bcyclo dextrin-containing PVA membrane. Mater. Sci. Eng. C **26**, 222–226 (2006)
13. J. Li, D. Kuang, Y. Feng, F. Zhang, Z. Xu, M. Liu, A graphene oxide-based electro chemical sensor for sensitive determination of 4-nitrophenol. J. Hazard. Mater. **201–202**, 250–259 (2012)
14. Y. Xu, Y. Wang, Y. Ding, L. Luo, X. Liu, Y. Zhang, Determination of p-nitro phenol on carbon paste electrode modified with a nanoscaled compound oxide Mg (Ni) FeO. J. Appl. Electrochem. **43**, 679–687 (2013)
15. Y.L. Yang, B. Unnikrishnan, S.M. Chen, Amperometric determination of 4- nitro phenol at multi-walled carbon nanotube-poly(diphenylamine) composite modified glassy carbon electrode. Int. J. Electrochem. Sci. **6**, 3902–3912 (2011)
16. H. Yin, Q. Ma, Y. Zhou, S. Ai, L. Zhu, Electrochemical behavior and voltammetric determination of 4-aminophenol based on graphene–chitosan composite film modified glassy carbon electrode. Electrochim. Acta **55**, 7102–7108 (2010)
17. L.Q. Luo, X.L. Zou, Y.P. Ding, Q.S. Wu, Derivative voltammetric direct simultane- ous determination of nitrophenol isomers at a carbon nanotube modified electrode. Sens. Actuators B **135**, 61–65 (2008)
18. L. Chu, L. Han, X. Zhang, Electrochemical simultaneous determination of nitro phenol isomers at nano-gold modified glassy carbon electrode. J. Appl. Electrochem. **41**(6), 687–694 (2011)
19. I.G. Casella, M. Contursi, The electrochemical reduction of nitrophenols on silver globular particles electrodeposited under pulsed potential conditions. J Electron. Chem. Soc. **154**, D697–D702 (2007)
20. W. Sun, M.X. Yang, Q. Jiang, K. Jiao, Direct electrocatalytic reduction of p-nitro phenol at room temperature ionic liquid modified electrode. Chin. Chem. Lett. **19**, 1156–1158 (2008)
21. X. Xie, Y. Li, Z. Liu, M. Haruta, W. Shen, Low-temperature oxidation of CO catalysed by Co_3O_4 nanorods. Nature **458**(7239), 746–749 (2009)
22. I. Celardo, J.Z. Pedersen, E. Traversa, L. Ghibelli, Pharmacological potential of cerium oxide nanoparticles. Nanoscale **3**, 1411–1420 (2011)
23. X.Q. Liu, J. Iocozzia, Y. Wang, X. Cui, Y.H. Chen, S.Q. Zhao, Z. Li, Z.Q. Lin, Noble metal-metal oxide nanohybrids with tailored nanostructures for efficient solar energy conversion, photocatalysis and environmental remediation. Energy Environ. Sci. **10**, 402–434 (2017)

24. N.R. Elezovic, B.M. Babic, V.R. Radmilovic, S.L. Gojkovic, N.V. Krstajic, L.M. Vracar, Pt/C doped by MoOx as the electrocatalyst for oxygen reduction and methanol oxidation. J. Power Sources **175**, 250–255 (2008)
25. Y. Bai, J. Wu, J. Xi, J. Wang, W. Zhu, L. Chen, X. Qiu, Electrochemical oxidation of ethanol on Pt–ZrO_2/C catalyst. Electrochem. Commun. **7**, 1087–1090 (2005)
26. L. Feng, J. Yang, Y. Hu, J. Zhu, C. Liu, W. Xing, Electrocatalytic properties of Pd CeOx/C anodic catalyst for formic acid electrooxidation. Int. J. Hydrog Energy **37**, 4812–4818 (2012)
27. C. Zhang, F. Meng, L. Wang, M. Zhang, Z. Ding, Morphology-selective synthesis method of gear-like CeO_2 microstructures and their optical properties. Mater. Lett. **130**, 202–205 (2014)
28. C.R. Li, Q.T. Sun, N.P. Lu, B.Y. Chen, W.J. Dong, A facile route for the fabrication of CeO_2 nanosheets via controlling the morphology of $CeOHCO_3$ precursors. J. Cryst. Growth **343**, 95–100 (2012)
29. R. Rao, M. Yang, Q. Ling, Q. Zhang, H. Liu, A. Zhang, W. Chen, Mesoporous CeO_2 nanobelts synthesized by a facile hydrothermal route via controlling cationic type and concentration of alkali. Microporous Mesoporous Mater. **169**, 81–87 (2013)
30. F. Niu, D. Zhang, L. Shi, X. He, H. Li, H. Mai, T. Yan, Facile synthesis, characteri- zation and low-temperature catalytic performance of Au/CeO_2 nanorods. Mater. Lett. **63**, 2132–2135 (2009)
31. K. Singh, A.A. Ibrahim, A. Umar, A. Kumar, G.R. Chaudhary, S. Singh, S.K. Mehta, Synthesis of CeO_2–ZnO nanoellipsoids as potential scaffold for the efficient detection of 4-nitrophenol. Sens. Actuators B **202**, 1044–1050 (2014)
32. C.R. Michel, A.H.M. Preciado, CO sensor based on thick films of 3D hierarchical CeO_2 architectures. Sens. Actuators B **197**, 177–184 (2014)
33. N.F. Hamedani, A.R. Mahjoub, A.A. khodadadi, Y. Mortazavi, CeO_2 doped ZnO flower-like nanostructure sensor selective to ethanol in presence of CO and CH_4. Sens. Actuators B **169**, 67–73 (2012)
34. S.K. Jha, C.N. Kumar, R.P. Raj, N.S. Jha, S. Mohan, Synthesis of 3D porous CeO_2/reduced graphene oxide xerogel composite and low level detection of H_2O_2. Electrochim. Acta **120**, 308–313 (2014)
35. A. Rahim, R.A. Hameed, M. Khalil, Nickel as a catalyst for the electro-oxidation of methanol in alkaline medium. J. Power Sources **134**, 160–169 (2004)
36. C. Fan, D. Piron, A. Sleb, P. Paradis, Study of electrodeposited nickel molybdenum, nickel tungsten, cobalt molybdenum, and cobalt tungsten as hydrogen electr odes in alkaline water electrolysis. J. Electrochem. Soc. **141**, 382–387 (1994)
37. M. Ranjbar, M.A. Taher, A. Sam, Mg-MOF-74 nanostructures: facile synthesis and characterization with aid of 2,6-pyridinedicarboxylic acid ammonium. J. Mater. Sci.: Mater. Electron. **27**(2), 1449–1456 (2016)
38. M. Ranjbar, M.S. Niasari, S.M.H. Mashkani, K.V. Rao, Solvothermal synthesis and characterization of hollow sphere-like ZnS/$ZnAl_2S_4$ nanocomposites. J. Inorg. Organomet. Polym. Mater. **22**(5), 1122–1127 (2012)
39. P. Rajaei, M. Ranjbar, Synthesis and characterization of zinc oxide nano structures by green capping agent and its photocatalytic degradation of methylene blue (MB). J. Mater. Sci.: Mater. Electron. **27**(2), 1708–1712 (2016)
40. M. Ranjbar, M.A. Taher, A. Sam, NiO nanostructures: novel solvent-less solid-state synthesis, characterization and MB photocatalytic degradation. J. Mater. Sci.: Mater. Electron. **26**(10), 8029–8034 (2015)
41. F. Sedighi, M.E. Zare, A.S. Nasab, M. Behpour, Synthesis and characterization of $CuWO_4$ nanoparticle and $CuWO_4$/NiO nanocomposite using co-precipitation method; application in photodegradation of organic dye in water. J. Mater. Sci.: Mater. Electron. **29**(16), 13737–13745 (2018)
42. M.R. Nasrabadi, M. Behpour, A.S. Nasab, M.R. Jeddy, Nanocrystalline Ce-doped copper ferrite: synthesis, characterization, and its photocatalyst application. J. Mater. Sci.: Mater. Electron. **27**(11), 11691–11697 (2016)
43. A.S. Nasab, S. Pourmasoud, F. Ahmadi, M. Wysokowski, T. Jesionowski, H. Ehrlich, M.R. Nasrabadi, Synthesis and characterization of $MnWO_4$/$TmVO_4$ ternary nano-hybrids by an ultrasonic method for enhanced photocatalytic activity in the degradation of organic dyes. Mater. Lett. **238**, 159–162 (2019)
44. H. Naderi, H. Sobati, A.S. Nasab, M.R. Nasrabadi, M.E. Arani, M.R. Ganjali, H. Ehrlich, Synthesis and supercapacitor application of cerium tungstate nano structure. Chem. Select **4**(10), 2862–2867 (2019)
45. S.M. Pourmortazavi, M.R. Nasrabadi, A.S. Nasab, M.S. Karimi, M.R. Ganjali, S. Mirsadeghi, Electrochemical synthesis of copper carbonates nano particles through experimental design and the subsequent thermal decomposition to copper oxide. Mater. Res. Express. **6**(4), 045065 (2019)
46. A.S. Nasab, M.R. Nasrabadi, H.R. Naderi, V. Pourmohamadian, F. Ahmadi, M.R. Ganjali, H. Ehrlich, Sonochemical synthesis of terbium tungstate for develo ping high power supercapacitors with enhanced energy densities. Ultrason. Sonochem **45**, 189–196 (2018)
47. D. Patil, N.Q. Dung, H. Jung, S.Y. Ahn, D.M. Jang, D. Kim, Enzymatic glucose bio sensor based on CeO_2 nanorods synthesized by non-isothermal precipitation. Biosens. Bioelectron. **31**, 176–181 (2012)
48. H. Yan, D. Zhang, J. Xu, Y. Lu, Y. Liu, K. Qiu, Y. Zhang, Y. Luo, Solution growth of NiO nanosheets supported on Ni foam as high performance electrodes for Super capacitors. Nanoscale Res. Lett. **9**, 424 (2014)
49. R. Wahab, A. Umar, S. Dwivedi, K.J. Tomar, H.S. Shin, I.H. Hwang, ZnO nano particles: cytological effect on chick fibroblast cells and antimicrobial activities towards *Escherichia coli* and *Bacillus subtilis*. Sci. Adv. Mater. **5**, 1571–1580 (2013)
50. L. Chen, L. Li, G. Li, Synthesis of CuO nanorods and their catalytic activity in the thermal decomposition of ammonium perchlorate. J. Alloys Compd. **464**, 532–536 (2008)
51. E. Kumar, P. Selvarajan, K. Balasubramanian, Preparation and studies of cerium dioxide (CeO_2) nanoparticles by microwave-assisted solution method. Recent Res. Sci. Technol. **2**, 37–41 (2010)
52. Y. Li, X. Liu, J. Li, Preparation and characterization of CeO_2 doped ZnO nano-tubes fluorescent composite. J. Rare Earth **28**, 571–575 (2010)
53. T. Ahmad, K.V. Ramanujachary, S.E. Lofland, A.K. Ganguli, Magnetic and electro chemical properties of nickel oxide nanoparticles obtained by the reverse-micellar route. Solid State Sci. **8**(42), 5–430 (2006)
54. X.M. Ni, Q.B. Zhao, B.B. Li, J. Cheng, H.G. Zheng, Interconnected β-$Ni(OH)_2$ sheets and their morphology-retained transformation into mesostructured Ni. Solid State Commun. **137**, 585–588 (2006)
55. X. Li, J. Li, D. Huo, Z. Xiu, X. Sun, Facile synthesis under near-atmospheric conditions and physicochemical properties of hairy CeO_2 nanocrystallines. J. Phys. Chem. C **113**, 1806–1811 (2009)
56. S.J. Gregg, K.S.W. Sing, *Adsorption, surface area and porosity* (Academic Press, London, 1982)

57. S. Lowell, J.E. Shields, *Powder surface area and porosity* (Chapman and Hall, London, 1984)
58. G. Wang, Y. Bao, Y. Tian, J. Xia, D. Cao, Electrocatalytic activity of perovskite La1-xSrx MnO_3 towards hydrogen peroxide reduction in alkaline medium. J. Power Sources **195**, 6463–6467 (2010)
59. N.Q. Dung, D. Patil, H. Jung, J. Kim, D. Kim, NiO-decorated single-walled carbon nanotubes for high-performance nonenzymatic glucose sensing. Sens. Actuators B **183**, 381–387 (2013)